

Aluminum Borohydride Complex with Ethylenediamine: Crystal Structure and Dehydrogenation Mechanism Studies

Qinfen Gu,^{*,†} Zhiyang Wang,^{†,‡} Yaroslav Filinchuk,[§] Justin A. Kimpton,[†] Helen E. A. Brand,[†] Qian Li,^{*,||,⊥} and Xuebin Yu[#]

[†]Australian Synchrotron, 800 Blackburn Road, Clayton 3168, Australia

[‡]School of Materials Science and Engineering, UNSW Australia, Sydney, 2052, Australia

[§]Institute of Condensed Matter and Nanosciences, Université Catholique de Louvain, Place L. Pasteur 1, 1348 Louvain-la-Neuve, Belgium

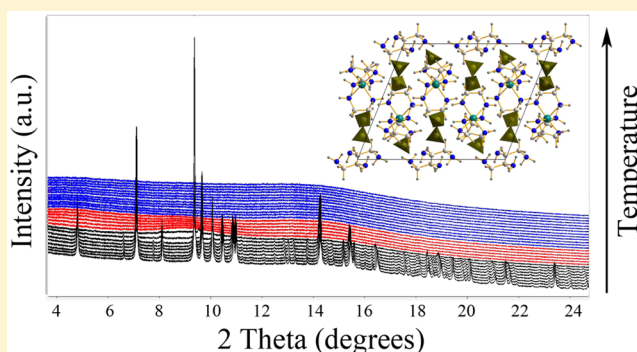
^{||}State Key Laboratory of Advanced Special Steel & Shanghai Key Laboratory of Advanced Ferrometallurgy & School of Materials Science and Engineering, Shanghai University, Shanghai 200072, China

[⊥]Institute of Genomic Material, Shanghai University, Shanghai 200444, China

[#]Department of Materials Science, Fudan University, Shanghai 200433, China

Supporting Information

ABSTRACT: We report the structure of an aluminum borohydride ethylenediamine complex, $\text{Al}(\text{EDA})_3 \cdot 3\text{BH}_4 \cdot \text{EDA}$. This structure was successfully determined using X-ray powder diffraction and was supported by first-principles calculations. The complex can be described as a mononuclear complex exhibiting three-dimensional supramolecular structure, built from units of $\text{Al}[\text{C}_2\text{N}_2\text{H}_8]_3$, BH_4 , and ethylenediamine (EDA) molecules. Examination of the chemical bonding indicates that this arrangement is stabilized via dihydrogen bonding between the NH_2 ligand in EDA and the surrounding BH_4 . The partial ionic bonding between the Al and N atoms in EDA forms a five-member ring (5MR), an $\text{Al}[\text{NCCN}]$ unit. The calculated H_2 removal energies confirm that it is energetically favorable to remove the loosely bonded EDA and H atoms with $\text{N}-\text{H} \cdots \text{H}-\text{B}$ dihydrogen bonds upon heating. Our results suggest that the NH_2 terminal ligand in the EDA molecule combines with a H atom in the BH_4 group to release H_2 at elevated temperature, and our results confirm that the experimental result $\text{Al}(\text{EDA})_3 \cdot 3\text{BH}_4 \cdot \text{EDA}$ can release 8.4 wt % hydrogen above 149 °C with detectable EDA molecules. This work provides insights into the dehydrogenation behavior of $\text{Al}(\text{EDA})_3 \cdot 3\text{BH}_4 \cdot \text{EDA}$ and has implications for future development of promising high-performance metal borohydride ethylenediamine complexes.



1. INTRODUCTION

With the increasing demand for renewable energy, people consider hydrogen as one of the suitable candidate energy carriers because it is environment friendly and abundant in earth. Recently, mass production of hydrogen fuel cell family vehicles has been achieved by several companies with ongoing large investments in this infrastructure. However, an efficient method to utilize safe and high density hydrogen storage in hydrogen vehicle applications is still a key challenge.^{1–3} Great interest has been focused on light complex metal hydrides such as metal hydrides, amides, and borohydrides for hydrogen storage. Among these materials, metal borohydrides such as LiBH_4 ,^{4,5} $\text{Mg}(\text{BH}_4)_2$,^{6,7} and $\text{Al}(\text{BH}_4)_3$ ^{8,9} are considered as promising materials because they have attractive properties of high volumetric and gravimetric hydrogen densities. As an example, $\text{Al}(\text{BH}_4)_3$ ^{8,9} possesses a theoretical gravimetric hydrogen density of 16.9 wt %, which reaches the system target of 5.5 wt % for 2017 set by the U.S. DOE.¹⁰ However,

dehydrogenation temperatures of metal borohydrides usually happen at over 250 °C and produce impurity gases, such as diborane, together with hydrogen,¹¹ which is inappropriate to be used in hydrogen fuel cell vehicles.

To overcome the kinetic and thermodynamic limitations of the decomposition of metal borohydrides, several strategies like catalytic doping,¹² nanoengineering,¹³ and additive destabilization¹⁴ have been employed in recent years. Additionally, the high stability of metal borohydrides can be tuned by the formation of bimetallic borohydrides, such as $\text{Al}_3\text{Li}_4(\text{BH}_4)_{13}$,¹⁵ $\text{LiZn}_2(\text{BH}_4)_5$,¹⁶ and $\text{NaZn}(\text{BH}_4)_3$.¹⁷ Their stability can be decreased with increased Pauling electronegativity (χ_p) of the metal cations in the structures, which weakens the B–H bonds with metal cations. However, these methods do not solve the

Received: March 13, 2016

Revised: April 20, 2016

Published: April 20, 2016

problem of undesired B₂H₆ gas generation during decomposition. On the other hand, complexes combined with ammonia borane (AB) and metal borohydride ammoniates (MBAs) have been developed. One of the fascinating strategies in the development of these compounds is trying to formulate the borohydrides with groups of H^{δ+} enriched molecules such as NH₃ to form novel nitrogen and boron-combined materials.¹⁸ Both hydridic and protic hydrogen atoms are contained in these compounds; as the result, they are proposed to release hydrogen under much milder conditions. Upon heating, a local combination of the N–H^{δ+}...H^{δ-}–B dihydrogen bonds can be realized in these compounds.¹⁹ For example, a series of MBAs, including LiBH₄·NH₃,^{20,21} Mg(BH₄)₂·2NH₃,²² and Al(BH₄)₃·*n*NH₃,²³ have been synthesized and studied as potential hydrogen storage materials. In these examples, compounds of Al–B–N–H systems are considered as one of the promising materials in terms of dehydrogenation properties. Compared to the high decomposition temperatures of the aluminum borohydrides, the aluminum ammoniate complex showed much lower decomposition temperature, together with a higher hydrogen purity.²⁴ Despite the high hydrogen content of AB (19.6 wt %), simple ammonia borane decomposed with only 6.5 wt % H₂ released, and decomposition was accompanied by borazine and amino-borane. A remarkable example of the dehydrogenation of AB on the Al³⁺ template is observed for the [Al(NH₃BH₃)(BH₄)₃] complex.²⁵ The endothermic release of two equivalents of hydrogen leads to the formation of [Al(NHBH₃)(BH₄)₃]_{*n*}, where the dehydrogenated ammonia borane remains coordinated to the Al atom. In the other group containing AB molecules, ammonia borane metal containing derivatives (MABs), such as LiNH₂BH₃ and NaLi(NH₂BH₃)₂, were synthesized with considerable improvement in performance, but still most of these MABs release toxic ammonia and NH₂BH₂ in addition to hydrogen.^{26,27}

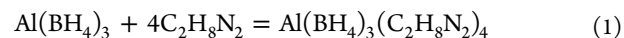
Recently, the ethylenediamine (EDA) containing complexes were explored because of their high hydrogen capacity.^{28,29} The EDA molecule is the simplest diamine and one of the fundamental chelating agents for coordination compounds. It is rich in protic hydrogen atoms. These EDA containing complexes can be considered as a potential chemical hydrogen storage material. It was demonstrated that some of the metal borohydride ethylenediamine complexes (labeled as EMBs) released traces of EDA molecules under decomposition, while the rest of the complexes can generate high purity hydrogen under similar conditions. The different decomposition behavior of these materials may be due to the different metal–ligand coordination strength because of the molecular and crystal structures; electronegativity of these compounds is different, which affects the chemical bonding properties among the Mg, Al, and BH₄ metal cations and EDA molecules and which thus leads to different dehydrogenation behavior. However, the structure of Al(BH₄)₃·*n*EDA complexes remained unresolved in the previous study.²⁹ Therefore, to understand the mechanism of the decomposition behavior of aluminum borohydride ethylenediamines requires detailed studies of the relationship of the crystal and electronic structures of the material in order to allow targeted design of these materials to further improve the dehydrogenation performance.

In this paper, Al(EDA)₃·3BH₄·EDA was synthesized via a direct synthesis approach on the basis of a gas–gas phase reaction between Al(BH₄)₃ and EDA. The compound has a theoretical hydrogen capacity of 14.2 wt %. The structure of

Al(EDA)₃·3BH₄·EDA was successfully solved from synchrotron powder X-ray diffraction (PXRD) data and was supported by first-principles calculations. The thermal decomposition behavior of this compound was studied with in situ high temperature PXRD measurements and was systematically compared with pristine aluminum borohydride through structural analysis and property evaluations. Meanwhile, the energies of dehydrogenation and the removal energies of EDAs in Al(EDA)₃·3BH₄·EDA were calculated.

2. EXPERIMENTAL DETAILS

2.1. Synthesis. The starting materials of LiBH₄ (95%), AlCl₃ (99.9%), and ethylenediamine (EDA) (99.5%) were obtained from Sigma-Aldrich and were used directly without further purification. First, Al(BH₄)₃ was obtained by the reaction of LiBH₄ and AlCl₃ under a flowing stream of high-purity Ar according to the reported method.³⁰ Then, synthesis of the Al(EDA)₃·3BH₄·EDA compound was realized by eq 1, using Al(BH₄)₃ gas phase with excessive EDA gas, similar to the method described in a previous report.²⁹



White powder was produced at the bottom of the reactor, and the excess EDA was removed with a roughing pump. The final solid product was examined with powder X-ray diffraction (PXRD) for structure, crystallinity, and phase purity analyses.

2.2. Diffraction Studies. PXRD experiments were conducted at the Powder Diffraction beamline, Australian Synchrotron. The as-produced fine white powder samples were packed into predried 0.7 mm boron–silica glass capillaries inside an argon-filled glovebox which was then sealed with vacuum grease for the measurements. An X-ray beam of a wavelength of 1.0315 Å was used in conjunction with a Mythen-II detector to collect the diffraction data. To estimate the dehydrogenation pathway and to identify the reaction products, time-resolved in-situ measurements were carried out with the capillary sample assembled in an in-house designed flow cell and heated using a Cyberstar hot-air blower. The sample was kept under 1 atm of high purity Ar atmosphere (99.999%) during heating from 30 to 300 °C in steps of 10 °C at a constant ramping rate of 6 °C/min. Diffraction data at each temperature step were collected over approximately 120 s.

3. FIRST-PRINCIPLES CALCULATIONS

Density functional theory (DFT) calculations were performed on the experimental structure using the CASTEP 8.0 software.³¹ The generalized gradient approximation (GGA)³² based on a Perdew–Burke–Ernzerhof (PBE) exchange correlation function³³ was used. The interactions between the ionic core and the valence electrons were treated with ultrasoft pseudopotentials.³⁴ Atomic pseudopotentials performed for atoms in this work corresponded to Al 3s²3p¹, B 2s²2p¹, N 2s²2p³, C 2s²2p², and H 1s¹. DFT-D semiempirical correction method represented by the Tkatchenko–Scheffler (TS) scheme³⁵ was used to account for hydrogen bonding and van der Waals (VdW) interactions. The cutoff energy of the plane wave basis set was 400 eV in all calculations, and Monkhorst Pack *k*-point mesh was used in the calculation to ensure that the total energy value convergence was within 1 meV/atom. During the optimization process, the tolerance convergence accuracy was set when the total energy was less than 2.0 × 10^{−6} eV/atom, the maximum force on each atom was less than 0.01

eV/nm, the maximum stress was less than 0.01 GPa, and the maximum displacement between cycles was less than 1×10^{-5} eV. DFT optimization of the structural model was performed with relaxed lattice parameters and atomic positions without space group symmetry constraints. The hydrogen and EDA removal energy calculations in $\text{Al}(\text{EDA})_3 \cdot 3\text{BH}_4 \cdot \text{EDA}$ were performed in a $2 \times 2 \times 2$ supercell to avoid unphysical interactions between neighbor cells and to make the computational results comparable. Isolated H_2 or EDA molecule energy was calculated in a $15 \times 15 \times 15 \text{ \AA}^3$ cubic cell.

4. RESULTS AND DISCUSSION

4.1. Crystal Structure Analysis. Figure 1 shows the Rietveld refinement of the synthesized sample using high-

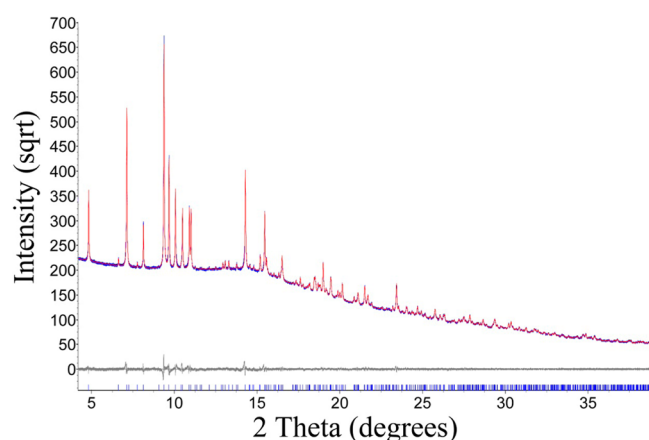


Figure 1. Rietveld refinement profile for $\text{Al}(\text{EDA})_3 \cdot 3\text{BH}_4 \cdot \text{EDA}$ phase showing observed (blue), calculated (red), and difference (gray) plots. The allowed Bragg reflections (tick marks) are shown for $\text{Al}(\text{EDA})_3 \cdot 3\text{BH}_4 \cdot \text{EDA}$ (blue).

resolution PXRD data. All diffraction peaks can be indexed in the high-resolution PXRD pattern suggesting that the reaction proceeded successfully and that a pure substance was obtained. Bragg peaks in the room temperature diffraction patterns from the sample were indexed to a monoclinic unit cell using code DICVOL06.³⁶ The structure was subsequently solved in the space group of $P2_1/a$ (No. 14) by global optimization in direct space, using the program FOX.³⁷ Different models were attempted, and finally, a model with the $[\text{Al}(\text{EDA})_3]^{3+}$ complex combined with one free EDA and three independent BH_4^- anions yielded a satisfactory solution. A good fit and several dihydrogen bonds with appropriate geometry confirmed the assumptions made. Rietveld refinement was performed using TOPAS v4.2 (Bruker 2008), and the refined lattice parameters are $a = 15.6538(5) \text{ \AA}$, $b = 11.2713(3) \text{ \AA}$, $c = 13.1701(4) \text{ \AA}$, $\beta = 111.7985(13)^\circ$, and $V = 2157.57(12) \text{ \AA}^3$. Because of the weak scattering of H atoms from PXRD data, the structure was refined with the BH_4 and EDA groups as relaxed rigid bodies with nominal bond distances as starting values. The diffraction profile fit is shown in Figure 1, with the agreement factors of $R_{\text{wp}} = 3.64\%$, $R_{\text{B}} = 2.56\%$, and $\text{GoF} = 1.883$. The results of the structure determination, experimental details, and atomic positions are presented in Table 1 and Table S1. First-principles calculations were then performed to search and validate the lowest energy structure configuration. More details can be found in the CIF file (CCDC 1463851).

The crystal structure of $\text{Al}(\text{EDA})_3 \cdot 3\text{BH}_4 \cdot \text{EDA}$, shown along the b axis in Figure 1a, can be described as a mononuclear

Table 1. Experimental and Crystallographic Details for $\text{Al}(\text{EDA})_3 \cdot 3\text{BH}_4 \cdot \text{EDA}$

formula sum	C32 N32 H176 B12 Al4
formula weight	1247.61 g/mol
crystal system	monoclinic
space group	$P2_1/a$ (14)
cell parameters	$a = 15.6538(5) \text{ \AA}$ $b = 11.2713(3) \text{ \AA}$ $c = 13.1701(4) \text{ \AA}$ $\beta = 111.7985(13)^\circ$
cell volume	$2157.57(12) \text{ \AA}^3$
Z	4
calcd density	0.9601 g/cm^3
R_{B}	2.56%
R_{wp}	3.64%
GoF	1.883
2θ	$2\theta_{\text{min}} = 3^\circ$; $2\theta_{\text{max}} = 83^\circ$
measured temperature	$26 \text{ }^\circ\text{C}$
diffractometer	Mythen-II

complex exhibiting three-dimensional supramolecular structure, which comprises building units of $[\text{C}_2\text{N}_2\text{H}_8]_3$, BH_4 , and ethylenediamine (EDA) molecules. The structure is associated together by $\text{H} \cdots \text{H}$ bonds between $[\text{Al}(\text{EDA})_3]^{3+}$, EDA, and BH_4 groups. Each Al^{3+} cation is linked via six N atoms to three chemically equivalent EDA molecules to form an octahedrally coordinated complex as shown in Figure 2b. Each surrounding EDA molecule has lone pairs on two N atoms, which form chelate $[\text{AlNCCN}]$ five-member rings (SMR) with a central Al^{3+} cation. This stable coordination is commonly observed in many coordination polymers. Short $\text{H} \cdots \text{H}$ distances, namely, $1.658\text{--}1.745 \text{ \AA}$, form between hydrogen atoms in BH_4 groups and the NH_2 fragment in $[\text{Al}(\text{EDA})_3]^{3+}$ complexes. It is likely that dihydrogen bonds occur between the BH_4 and the $[\text{Al}(\text{EDA})_3]^{3+}$ groups to stabilize the crystal structure. The weak $\text{H} \cdots \text{H}$ bonds in the range of $1.968\text{--}2.203 \text{ \AA}$ between the noncoordinated EDA molecule and the BH_4 groups form zigzag chains along the a axis. Similar features were observed in the structures of $\text{Mg}(\text{BH}_4)_2 \cdot 3\text{EDA}$ and $\text{Mg}(\text{BH}_4)_2 \cdot 4\text{EDA}$.²⁸ In both these Mg containing compounds, a $[\text{Mg}(\text{EDA})_3]^{2+}$ complex formed with Mg–N distances of $2.21\text{--}2.24 \text{ \AA}$, which are much longer than Al–N distances ranging from 2.003 to 2.111 \AA in the $[\text{Al}(\text{EDA})_3]^{3+}$ complex. This indicates possible stronger bonding in the $[\text{Al}(\text{EDA})_3]^{3+}$ complex. Moreover, the structure of $\text{Mg}(\text{BH}_4)_3 \cdot 3\text{EDA}$ does not contain the non-coordinated EDA molecules.

4.2. Decomposition Pathway. The thermal decomposition behavior for $\text{Al}(\text{EDA})_3 \cdot 3\text{BH}_4 \cdot \text{EDA}$ sample measured with in situ PXRD is presented in Figure 3. The PXRD patterns show two separate decomposition steps from room temperature to $300 \text{ }^\circ\text{C}$. When the sample is heated from 30 to $100 \text{ }^\circ\text{C}$, the peak intensities are almost unchanged, while all diffraction peaks shift slightly to lower 2θ angles. This reveals that the unit cell increases slightly with temperature, and the material is stable in this temperature range. Starting from $110 \text{ }^\circ\text{C}$, peak intensities gradually decrease and no new peaks appear, indicating that the sample is partially decomposed but that no polymorphic phase transition occurs. At $150 \text{ }^\circ\text{C}$, all sharp peaks have totally disappeared, and the sample decomposes into an amorphous phase A with two broad bumps around 8.9 and 14.8° in the PXRD pattern. From $200 \text{ }^\circ\text{C}$, the broad bump around 8.9° disappears and only the broad bump around 14.5°

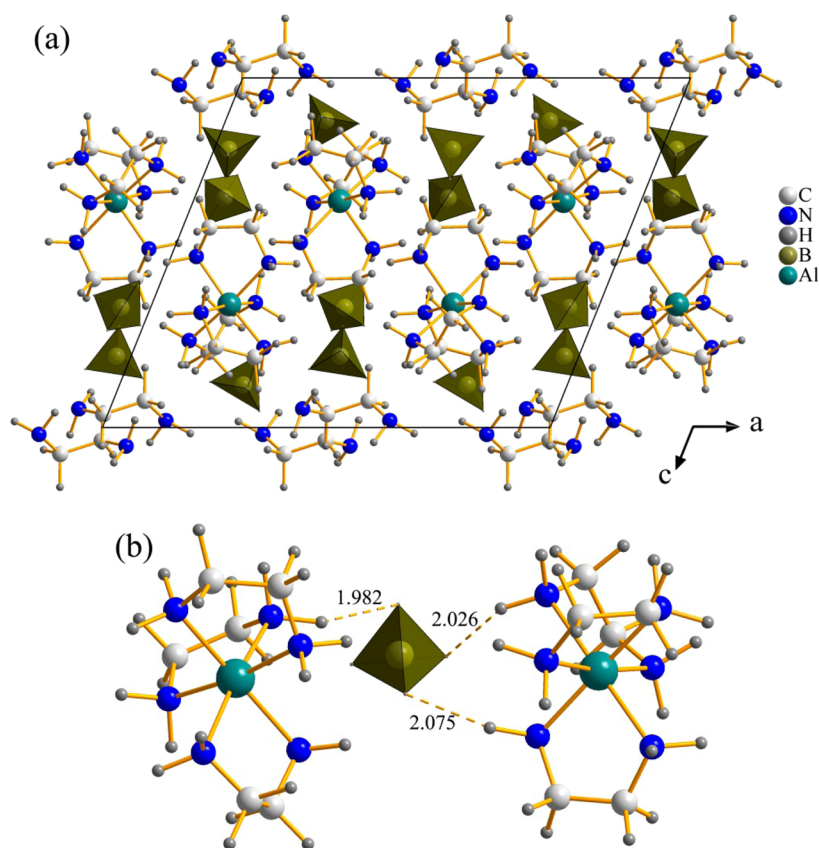


Figure 2. Three dimensional crystal structure of $\text{Al}(\text{EDA})_3 \cdot 3\text{BH}_4 \cdot \text{EDA}$ (a) presented in a unit cell viewing along b axis and (b) local atomic structure of $\text{Al}(\text{EDA})_3$ complex (Al^{3+} cation coordinates with three EDA molecules) with BH_4 group.

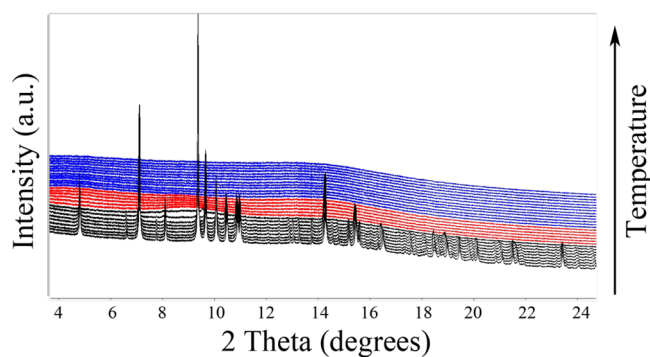


Figure 3. In-situ variable temperature synchrotron powder XRD of $\text{Al}(\text{EDA})_3 \cdot 3\text{BH}_4 \cdot \text{EDA}$ compound. Black lines show crystalline phase, red lines show amorphous phase A, and blue lines show higher temperature amorphous phase B.

remains. This indicates that amorphous phase A further decomposes into another amorphous phase B at higher temperatures. In the temperature range from 200 °C to the highest temperature measured in this study, 300 °C, no further significant change is observed in the PXRD patterns. Our results agree well with the reported differential scanning calorimetry (DSC) and thermal analysis/mass spectrometry (TG/MS) results, where two exothermic peaks were observed at 149 and 198 °C.²⁹ TG/MS analysis showed two dehydrogenation steps for the $\text{Al}(\text{EDA})_3 \cdot 3\text{BH}_4 \cdot \text{EDA}$ sample, with 4.8 wt % hydrogen released in the first step and 8.4 wt % hydrogen released in total. A trace amount of EDA was detected along with hydrogen generation of 96.1% H_2 purity.

Given the noncoordinated weakly $\text{H} \cdots \text{H}$ bonded EDA with surrounding BH_4 groups in the structure, it is expected that this EDA can easily detach from the structure upon heating.

4.3. Chemical Bond Analysis. To understand the bonding character and decomposition mechanism of $\text{Al}(\text{EDA})_3 \cdot 3\text{BH}_4 \cdot \text{EDA}$ compound, we employed first-principles calculations to investigate the optimized crystal structure, electronic structure, and thermodynamic properties of decomposition, including the energies of dehydrogenation and the removal energies of EDA molecules in $\text{Al}(\text{EDA})_3 \cdot 3\text{BH}_4 \cdot \text{EDA}$. For comparison, a pristine aluminum borohydride compound, $\beta\text{-Al}(\text{BH}_4)_3$, was also calculated, for which the crystal structures and calculated data are shown in Figure S1 and Table S2. The calculated lattice parameters for $\text{Al}(\text{EDA})_3 \cdot 3\text{BH}_4 \cdot \text{EDA}$ are in good agreement with the experimental data with about 3–4% difference, which shows the reliability of our calculation method. The calculated total and partial electronic density of states (DOS) for both compounds are shown in Figure 4. In general, there are finite energy gaps of 2.8 and 5.8 eV for $\text{Al}(\text{EDA})_3 \cdot 3\text{BH}_4 \cdot \text{EDA}$ and $\beta\text{-Al}(\text{BH}_4)_3$, respectively, which exhibit nonmetallic features. The actual gap could be even larger since DFT is known to underestimate the band gap of semiconductors and insulators. The calculated band gap, 2.8 eV, of $\text{Al}(\text{EDA})_3 \cdot 3\text{BH}_4 \cdot \text{EDA}$ is in the range of wide semiconductors (e.g., GaN 3.4 eV, GaP 2.26 eV) and is much narrower than that of $\beta\text{-Al}(\text{BH}_4)_3$. This implies that the coordination of the EDA groups narrows the band gap. The occupied states at E_F are mainly contributed by N and H atoms from EDA molecules. The lower valence band (VB) region (below -10 eV) is dominated by N 2s, C 2s, and H(EDA) 1s states; the upper VB (from -8 eV to E_F) is clearly

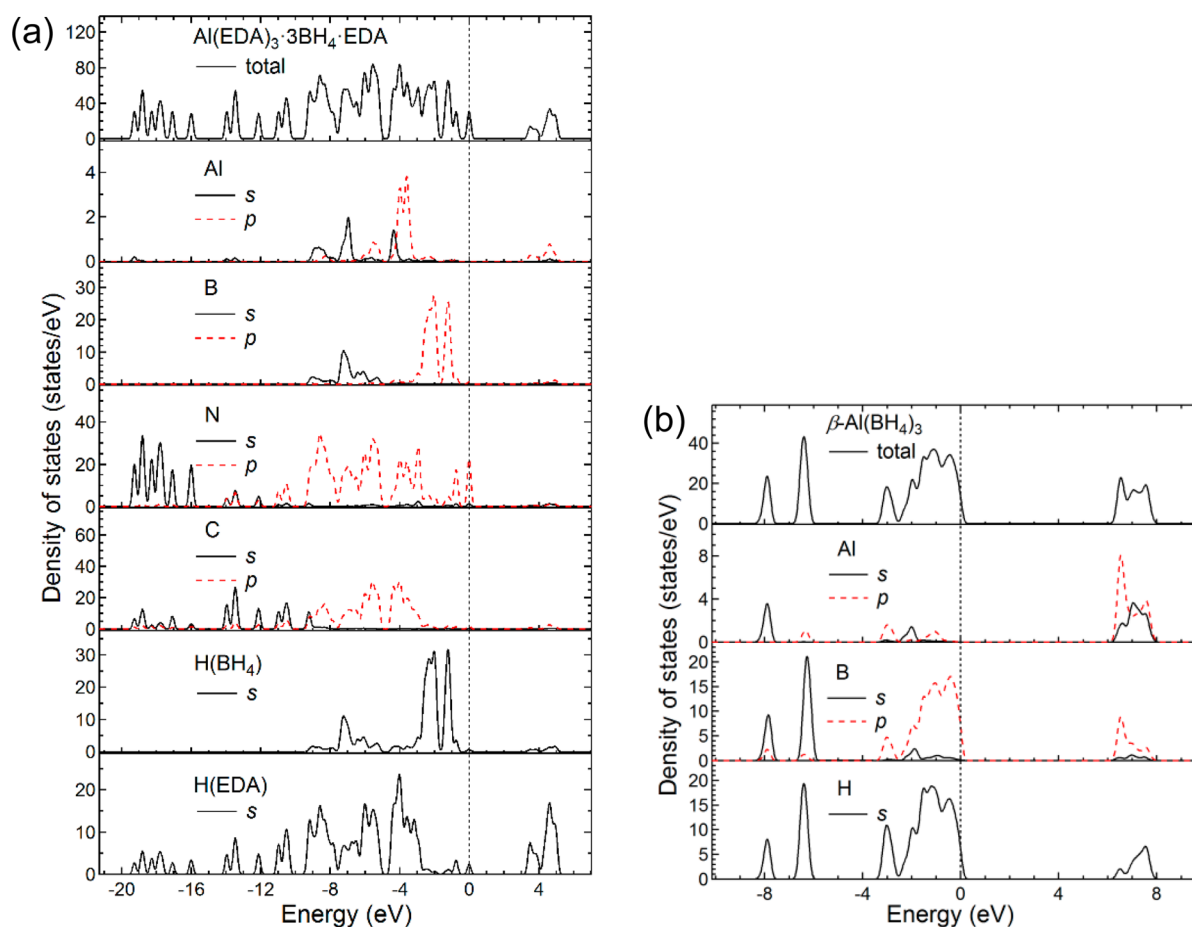


Figure 4. Total and partial electronic density of states for (a) $\text{Al}(\text{EDA})_3 \cdot 3\text{BH}_4 \cdot \text{EDA}$ and (b) $\beta\text{-Al}(\text{BH}_4)_3$. The Fermi level is set to 0 eV and marked as the vertical dash line.

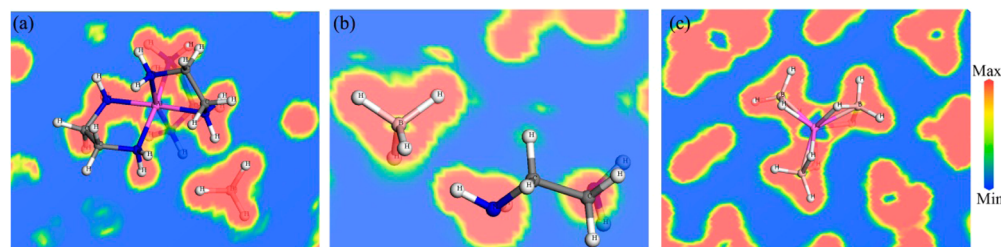


Figure 5. Electron localization function (ELF) for $\text{Al}(\text{BH}_4)_3 \cdot 4\text{EDA}$ and $\text{Al}(\text{BH}_4)_3$. 2D cross sections cut through Al (purple), B (pink), N (blue), and H (white) atoms (rainbow scale is used $\text{ELF}_{\min} = 0.02$, $\text{ELF}_{\max} = 0.9$).

indicated by strong *sp* hybridization of states among Al 3*p*, N 2*p*, and H(EDA) 1*s*. This may result in a strong association between the Al atom and the coordinated EDA molecules, stabilizing the structure. The top of VB is composed of B 2*p* and H(BH₄) 1*s* hybridized states, which reflects the picture in a tetrahedral unit like BH₄. Our calculated electronic DOS of $\beta\text{-Al}(\text{BH}_4)_3$ is similar to the results by Miwa et al.³⁸ The VB is well separated into two regions (from −9 to −6 eV and from −4 eV to E_{F}). The occupied states are primarily dominated by B 2*s*2*p* and H 1*s* orbitals, with negligible contribution from Al orbitals. This shows essentially ionic interaction between Al atoms and BH₄ groups.

The electronic structure was further analyzed by examining the valence electron localization function (ELF). ELF is based on the Hartree–Fock pair probability of parallel spin electrons and can be calculated in density functional theory from the

excess kinetic energy density because of Pauli repulsion.^{39,40} ELF can be used as an indicator for understanding the chemical bonding in solids. As shown in Figure 5, the large value of ELF at all H sites indicates either strongly paired electrons or closed-shell bonds. It can be seen in Figure 5a that the high ELF value between Al and N and the negligibly small value of ELF at the Al site with distorted square distribution shape indicate that the bonding interaction between Al and N is partially ionic. It shows that there is some charge transfer from Al to N atoms. The ELF distribution at the H site in BH₄ group is not spherically symmetric, and it is polarized toward the H atom in the $[\text{Al}(\text{EDA})_3]^{3+}$ group indicating the influence of the H···H bonding between the two groups. A similar ELF feature can be seen in Figure 5b, where the ELF distribution at the H site in the noncoordinated EDA group is distorted toward the neighboring BH₄ group. It indicates that the H···H bonding

also exists in between these two groups. In the case of $\text{Al}(\text{BH}_4)_3$, shown in Figure 5c, the negligibly small value of ELF at the Al site with distorted triangle distribution and the high ELF value in between Al and B atoms indicate the partially ionic bonding between Al and B atoms in the plane. It also shows strong Al–H bonding with high ELF value in between. This explains the decomposition of $\beta\text{-Al}(\text{BH}_4)_3$ at a high dehydrogenation temperature of about 250 °C with B_2H_6 as impurity.⁹

4.4. Dehydrogenation Mechanism. From the electronic structure analysis presented earlier, with the oppositely charged $\text{H}^{\delta+}$ from EDA units and $\text{H}^{\delta-}$ from BH_4 units in the crystal structure of $\text{Al}(\text{EDA})_3\cdot 3\text{BH}_4\cdot \text{EDA}$, the N–H \cdots H–B dihydrogen bonding occurs between the EDA and BH_4 units with the H \cdots H distance in the range of 1.658–2.203 Å. The intramolecular N–H \cdots H–B dihydrogen bonds may contribute to the recombination of $\text{H}^{\delta+}$ and $\text{H}^{\delta-}$ and may be the key to achieving the relatively low dehydrogenation temperature of $\text{Al}(\text{EDA})_3\cdot 3\text{BH}_4\cdot \text{EDA}$, 149 °C.²⁹ Two types of hydrogen atoms can be identified in the $\text{Al}(\text{EDA})_3\cdot 3\text{BH}_4\cdot \text{EDA}$: the H atoms in the EDA groups and the H atoms in the BH_4 groups. The initial step in the decomposition can be classified into two scenarios: (1) the noncoordinated EDA leaves the structure and (2) the combination of $\text{H}^{\delta+}$ and $\text{H}^{\delta-}$ from BH_4 and EDA, forming H_2 gas. These two proposed decomposition mechanisms were investigated by separately removing the EDA group or by removing the $\text{H}^{\delta+}$ and $\text{H}^{\delta-}$ from the BH_4 and EDA with the short distances. The removal energies can be calculated by using eq 2:

$$\Delta E = E_{\text{total}}(\text{EMB} - X) + E_{\text{total}}(X) - E_{\text{total}} \quad (2)$$

where E_{total} is the total energy of a $2 \times 2 \times 2$ supercell of $\text{Al}(\text{EDA})_3\cdot 3\text{BH}_4\cdot \text{EDA}$; $E_{\text{total}}(X)$ presents the energy of an isolated H_2 or EDA molecule; and $E_{\text{total}}(\text{EMB} - X)$ is the total energy of a supercell of $\text{Al}(\text{EDA})_3\cdot 3\text{BH}_4\cdot \text{EDA}$ after several X molecules have been removed. The calculated removal energies are listed in Table 2. By comparing the removal energies of four

Table 2. Removal Energies To Remove H_2 , EDA Molecule from a Supercell of $\text{Al}(\text{EDA})_3\cdot 3\text{BH}_4\cdot \text{EDA}$

removed molecule	energy (kJ/mol) (per formula unit)
2H(N–H \cdots H–B) the shortest H–H bond	217.462
2H(N–H \cdots H–B) 2nd shortest H–H bond	229.768
EDA (noncoordinated)	255.979
EDA ($\text{Al}[\text{C}_2\text{N}_2\text{H}_8]_3$)	407.363

types of molecules, we found that removing the noncoordinated EDA required a relatively low energy of 255.979 kJ/mol, which confirms that EDA molecule can be easily released. The removal energies of two different distance N–H \cdots H–B dihydrogen bonds are 217.462 and 229.768 kJ/mol, implying that their removals are the most energetically favorable. This suggests that the H atom in the NH_2 fragment of the EDA molecule combines with the H atom in the BH_4 group to release H_2 at elevated temperature. These H–H interactions are expected to have profound impacts on the thermal behavior of the $\text{Al}(\text{EDA})_3\cdot 3\text{BH}_4\cdot \text{EDA}$ compound. On the other hand, the removal energy for coordinated EDA in $[\text{Al}(\text{EDA})_3]^{3+}$ is much higher at 407.363 kJ/mol, suggesting that removing this group is energetically unfavorable while heating. The first main H_2 peak with 4.8 wt % hydrogen

released at 149 °C as shown in the MS results²⁹ is consistent with this N–H \cdots H–B dihydrogen bond mechanism. Between 150 and 180 °C, there was a 18.3 wt % drop from TG results, which corresponds to both noncoordinated EDA and the hydrogen being released within this temperature range. The earlier calculation results are in good agreement with reported experimental dehydrogenation data showing that 96.1% purity hydrogen can be released with EDA as the only detectable impurity gas.

5. CONCLUSION

In summary, the $\text{Al}(\text{EDA})_3\cdot 3\text{BH}_4\cdot \text{EDA}$ compound has been synthesized, which has a monoclinic crystal structure (space group $P2_1/a$) with lattice parameters $a = 15.6538(5)$ Å, $b = 11.2713(3)$ Å, $c = 13.1701(4)$ Å, $\beta = 111.7985(13)^\circ$, and volume of 2157.57(12) Å³. First-principles calculations were carried out to study the structural properties of the $\text{Al}(\text{EDA})_3\cdot 3\text{BH}_4\cdot \text{EDA}$ as a potential hydrogen storage material. The electronic structure of $\text{Al}(\text{EDA})_3\cdot 3\text{BH}_4\cdot \text{EDA}$ was analyzed via the electronic densities of states and the valence electron localization function analysis. The DOS and ELF analysis manifested strong correlation as N–H \cdots H–B dihydrogen bonds occur between NH_2 ligand in the EDA group and H atoms in the BH_4 group. The partial Al–N ionic bonding in $[\text{Al}(\text{EDA})_3]^{3+}$ is confirmed. The DFT calculation indicated that it has a band gap of 2.8 eV as a wide band gap semiconductor. The removal energies were further investigated to explain the dehydrogenation properties of $\text{Al}(\text{EDA})_3\cdot 3\text{BH}_4\cdot \text{EDA}$ compared to pristine $\beta\text{-Al}(\text{BH}_4)_3$. It was also illustrated that the N–H \cdots H–B dihydrogen bonding improves the dehydrogenation properties compared to the pristine $\beta\text{-Al}(\text{BH}_4)_3$. EDA coordination number and EDA/ BH_4 group ratio have significant impacts on decomposition mechanism, such as hydrogen capacity, purity, and dehydrogenation temperature. Our results would be illuminative for understanding the dehydrogenation behavior and the design of future metal borohydride ethylenediamine complexes.

■ ASSOCIATED CONTENT

Supporting Information

The Supporting Information is available free of charge on the ACS Publications website at DOI: 10.1021/acs.jpcc.6b02575.

Experimental atomic positions of $\text{Al}(\text{EDA})_3\cdot 3\text{BH}_4\cdot \text{EDA}$ and DFT calculated crystal structure details of $\text{Al}(\text{EDA})_3\cdot 3\text{BH}_4\cdot \text{EDA}$ and $\beta\text{-Al}(\text{BH}_4)_3$ compounds
(PDF)

■ AUTHOR INFORMATION

Corresponding Authors

*Tel: +61-3-85404219. E-mail: qinfen.gu@synchrotron.org.au.

*Tel: +86-21-66135659. E-mail: shuliqian@shu.edu.cn.

Notes

The authors declare no competing financial interest.

■ ACKNOWLEDGMENTS

Part of the experiment was performed at the PD beamline, Australian Synchrotron. Y. F. acknowledges support from FNRS (Belgium). Q. L. would like to thank the financial supports from the National Natural Science Foundation of China (51222402), “Shu Guang” project supported by Shanghai Municipal Education Commission and Shanghai Education Development Foundation (13SG39).

REFERENCES

- (1) Schlapbach, L.; Züttel, A. Hydrogen-Storage Materials for Mobile Applications. *Nature* **2001**, *414*, 353–358.
- (2) Züttel, A. Materials for Hydrogen Storage. *Mater. Today* **2003**, *6*, 24–33.
- (3) Rowsell, J. L. C.; Yaghi, O. M. Strategies for Hydrogen Storage in Metal-Organic Frameworks. *Angew. Chem., Int. Ed.* **2005**, *44*, 4670–4679.
- (4) Vajo, J. J.; Skeith, S. L.; Mertens, F. Reversible Storage of Hydrogen in Destabilized LiBh_4 . *J. Phys. Chem. B* **2005**, *109*, 3719–3722.
- (5) Züttel, A.; Rentsch, S.; Fischer, P.; Wenger, P.; Sudan, P.; Mauron, P.; Emmenegger, C. Hydrogen Storage Properties of LiBh_4 . *J. Alloys Compd.* **2003**, *356*, 515–520.
- (6) Chlopek, K.; Frommen, C.; Leon, A.; Zabara, O.; Fichtner, M. Synthesis and Properties of Magnesium Tetrahydroborate, $\text{Mg}(\text{Bh}_4)$ (2). *J. Mater. Chem.* **2007**, *17*, 3496–3503.
- (7) Soloveichik, G. L.; Gao, Y.; Rijssenbeek, J.; Andrus, M.; Kniajanski, S.; Bowman, R. C.; Hwan, S. J.; Zhao, J. C. Magnesium Borohydride as a Hydrogen Storage Material: Properties and Dehydrogenation Pathway of Unsolvated $\text{Mg}(\text{Bh}_4)$ (2). *Int. J. Hydrogen Energy* **2009**, *34*, 916–928.
- (8) Almennigen, A.; Gunderse, G.; Haaland, A. On Molecular Structure of Aluminium Borohydride $\text{Al}(\text{Bh}_4)_3$. *Acta Chem. Scand.* **1968**, *22*, 328–334.
- (9) Aldridge, S.; Blake, A. J.; Downs, A. J.; Gould, R. O.; Parsons, S.; Pulham, C. R. Some Tetrahydroborate Derivatives of Aluminium: Crystal Structures of Dimethylaluminium Tetrahydroborate and the [Small Alpha] and [Small Beta] Phases of Aluminium Tris-(Tetrahydroborate) at Low Temperature. *J. Chem. Soc., Dalton Trans.* **1997**, 1007–1012.
- (10) Klebanoff, L. E.; Keller, J. O. 5 Years of Hydrogen Storage Research in the Us Doe Metal Hydride Center of Excellence (Mhcoe). *Int. J. Hydrogen Energy* **2013**, *38*, 4533–4576.
- (11) Nakamori, Y.; Li, H. W.; Matsuo, M.; Miwa, K.; Towata, S.; Orimo, S. Development of Metal Borohydrides for Hydrogen Storage. *J. Phys. Chem. Solids* **2008**, *69*, 2292–2296.
- (12) Fan, M. Q.; Sun, L. X.; Zhang, Y.; Xu, F.; Zhang, J.; Chu, H. L. The Catalytic Effect of Additive Nb_2O_5 on the Reversible Hydrogen Storage Performances of $\text{LiBh}_4\text{-MgH}_2$ Composite. *Int. J. Hydrogen Energy* **2008**, *33*, 74–80.
- (13) Kojima, Y.; Suzuki, K.; Kawai, Y. Hydrogen Generation from Lithium Borohydride Solution over Nano-Sized Platinum Dispersed on LiCoO_2 . *J. Power Sources* **2006**, *155*, 325–328.
- (14) Li, H. W.; Kikuchi, K.; Nakamori, Y.; Miwa, K.; Towata, S.; Orimo, S. Effects of Ball Milling and Additives on Dehydrogenation Behaviors of Well-Crystallized $\text{Mg}(\text{Bh}_4)$ (2). *Scr. Mater.* **2007**, *57*, 679–682.
- (15) Lindemann, I.; Domenech-Ferrer, R.; Dunsch, L.; Filinchuk, Y.; Cerny, R.; Hagemann, H.; D'Anna, V.; Daku, L. M. L.; Schultz, L.; Gutfleisch, O. $\text{Al}_3\text{Li}_4(\text{Bh}_4)$ (13): A Complex Double-Cation Borohydride with a New Structure. *Chem. - Eur. J.* **2010**, *16*, 8707–8712.
- (16) Cerny, R.; Schouwink, P.; Sadikin, Y.; Stare, K.; Smrcok, L.; Richter, B.; Jensen, T. R. Trimetallic Borohydride $\text{Li}_3\text{Mn}_5(\text{Bh}_4)$ (15) ($M = \text{Mg}, \text{Mn}$) Containing Two Weakly Interconnected Frameworks. *Inorg. Chem.* **2013**, *52*, 9941–9947.
- (17) Cerny, R.; Kim, K. C.; Penin, N.; D'Anna, V.; Hagemann, H.; Sholl, D. S. $\text{Azn}(2)(\text{Bh}_4)$ (5) ($a = \text{Li}, \text{Na}$) and $\text{Nazn}(\text{Bh}_4)$ (3): Structural Studies. *J. Phys. Chem. C* **2010**, *114*, 19127–19133.
- (18) Gu, Q. F.; Gao, L.; Guo, Y. H.; Tan, Y. B.; Tang, Z. W.; Wallwork, K. S.; Zhang, F. W.; Yu, X. B. Structure and Decomposition of Zinc Borohydride Ammonia Adduct: Towards a Pure Hydrogen Release. *Energy Environ. Sci.* **2012**, *5*, 7590–7600.
- (19) Mao, J.; Gu, Q.; Guo, Z.; Liu, H. K. Sodium Borohydride Hydrazinates: Synthesis, Crystal Structures, and Thermal Decomposition Behavior. *J. Mater. Chem. A* **2015**, *3*, 11269–11276.
- (20) Guo, Y. H.; Xia, G. L.; Zhu, Y. H.; Gao, L.; Yu, X. B. Hydrogen Release from Amminelithium Borohydride, LiBh_4 Center Dot Nhh_3 . *Chem. Commun.* **2010**, *46*, 2599–2601.
- (21) Johnson, S. R.; David, W. I. F.; Royle, D. M.; Sommariva, M.; Tang, C. Y.; Fabbiani, F. P. A.; Jones, M. O.; Edwards, P. P. The Monoammoniate of Lithium Borohydride, $\text{Li}(\text{Nhh}_3)\text{Bh}_4$: An Effective Ammonia Storage Compound. *Chem. - Asian J.* **2009**, *4*, 849–854.
- (22) Soloveichik, G.; Her, J. H.; Stephens, P. W.; Gao, Y.; Rijssenbeek, J.; Andrus, M.; Zhao, J. C. Ammine Magnesium Borohydride Complex as a New Material for Hydrogen Storage: Structure and Properties of $\text{Mg}(\text{Bh}_4)$ (2)Center Dot 2nh_3 (3). *Inorg. Chem.* **2008**, *47*, 4290–4298.
- (23) Tang, Z. W.; Tan, Y. B.; Wu, H.; Gu, Q. F.; Zhou, W.; Jensen, C. M.; Yu, X. B. Metal Cation-Promoted Hydrogen Generation in Activated Aluminium Borohydride Ammoniates. *Acta Mater.* **2013**, *61*, 4787–4796.
- (24) Guo, Y. H.; Wu, H.; Zhou, W.; Yu, X. B. Dehydrogenation Tuning of Ammine Borohydrides Using Double-Metal Cations. *J. Am. Chem. Soc.* **2011**, *133*, 4690–4693.
- (25) Dovgaliuk, I.; Le Duff, C. S.; Robeyns, K.; Devillers, M.; Filinchuk, Y. Mild Dehydrogenation of Ammonia Borane Complexed with Aluminium Borohydride. *Chem. Mater.* **2015**, *27*, 768–777.
- (26) Ramzan, M.; Ahuja, R. Hybrid Density Functional and Molecular Dynamics Study of Promising Hydrogen Storage Materials: Double Metal Amidoboranes and Metal Amidoborane Ammoniates. *J. Phys. Chem. C* **2012**, *116*, 17351–17359.
- (27) Lee, T. B.; McKee, M. L. Mechanistic Study of LiNh_2bh_3 Formation from $\text{Li}(h)_4 + \text{Nh}_3\text{bh}_3$ and Subsequent Dehydrogenation. *Inorg. Chem.* **2009**, *48*, 7564–7575.
- (28) Chen, J.; Chua, Y. S.; Wu, H.; Xiong, Z. T.; He, T.; Zhou, W.; Ju, X. H.; Yang, M. H.; Wu, G. T.; Chen, P. Synthesis, Structures and Dehydrogenation of Magnesium Borohydride-Ethylenediamine Composites. *Int. J. Hydrogen Energy* **2015**, *40*, 412–419.
- (29) Zheng, X. F.; Huang, X. F.; Song, Y. Z.; Ma, X. H.; Guo, Y. H. Aluminium Borohydride-Ethylenediamine as a Hydrogen Storage Candidate. *RSC Adv.* **2015**, *5*, 105618–105621.
- (30) Schlesinger, H. I.; Brown, H. C.; Hyde, E. K. New Developments in the Chemistry of Diborane and of the Borohydrides 0.7. The Preparation of Other Borohydrides by Metathetical Reactions Utilizing the Alkali Metal Borohydrides. *J. Am. Chem. Soc.* **1953**, *75*, 209–213.
- (31) Clark, S. J.; Segall, M. D.; Pickard, C. J.; Hasnip, P. J.; Probert, M. J.; Refson, K.; Payne, M. C. First Principles Methods Using Castep. *Z. Kristallogr. - Cryst. Mater.* **2005**, *220*, 567–570.
- (32) Perdew, J. P.; Burke, K.; Ernzerhof, M. Generalized Gradient Approximation Made Simple. *Phys. Rev. Lett.* **1996**, *77*, 3865–3868.
- (33) Perdew, J. P.; Zunger, A. Self-Interaction Correction to Density-Functional Approximations for Many-Electron Systems. *Phys. Rev. B: Condens. Matter Mater. Phys.* **1981**, *23*, 5048–5079.
- (34) Vanderbilt, D. Soft Self-Consistent Pseudopotentials in a Generalized Eigenvalue Formalism. *Phys. Rev. B: Condens. Matter Mater. Phys.* **1990**, *41*, 7892–7895.
- (35) Tkatchenko, A.; Scheffler, M. Accurate Molecular Van Der Waals Interactions from Ground-State Electron Density and Free-Atom Reference Data. *Phys. Rev. Lett.* **2009**, *102*, 4.
- (36) Louer, D.; Boulitif, A. Indexing with the Successive Dichotomy Method, Dicvol04. *Zeitschrift Fur Kristallographie* **2006**, *2006*, 225–230.
- (37) Favre-Nicolin, V.; Cerny, R. Fox, 'Free Objects for Crystallography': A Modular Approach to Ab Initio Structure Determination from Powder Diffraction. *J. Appl. Crystallogr.* **2002**, *35*, 734–743.
- (38) Miwa, K.; Ohba, N.; Towata, S.-i.; Nakamori, Y.; Züttel, A.; Orimo, S.-i. First-Principles Study on Thermodynamical Stability of Metal Borohydrides: Aluminum Borohydride $\text{Al}(\text{Bh}_4)_3$. *J. Alloys Compd.* **2007**, *446–447*, 310–314.
- (39) Kohout, M. A Measure of Electron Localizability. *Int. J. Quantum Chem.* **2004**, *97*, 651–658.
- (40) Becke, A. D.; Edgecombe, K. E. A Simple Measure of Electron Localization in Atomic and Molecular Systems. *J. Chem. Phys.* **1990**, *92*, 5397–5403.